

An Organoid for Woven Bone

Anat Akiva,* Johanna Melke, Sana Ansari, Nalan Liv, Robin van der Meijden, Merijn van Erp, Feihu Zhao, Merula Stout, Wouter H. Nijhuis, Cilia de Heus, Claudia Muñiz Ortera, Job Fermie, Judith Klumperman, Keita Ito, Nico Sommerdijk,* and Sandra Hofmann*

Bone formation (osteogenesis) is a complex process in which cellular differentiation and the generation of a mineralized organic matrix are synchronized to produce a hybrid hierarchical architecture. To study the mechanisms of osteogenesis in health and disease, there is a great need for functional model systems that capture in parallel, both cellular and matrix formation processes. Stem cell-based organoids are promising as functional, self-organizing 3D *in vitro* models for studying the physiology and pathology of various tissues. However, for human bone, no such functional model system is yet available. This study reports the *in vitro* differentiation of human bone marrow stromal cells into a functional 3D self-organizing co-culture of osteoblasts and osteocytes, creating an organoid for early stage bone (woven bone) formation. It demonstrates the formation of an organoid where osteocytes are embedded within the collagen matrix that is produced by the osteoblasts and mineralized under biological control. Alike *in vivo* osteocytes, the embedded osteocytes show network formation and communication via expression of sclerostin. The current system forms the most complete 3D living *in vitro* model system to investigate osteogenesis, both in physiological and pathological situations, as well as under the influence of external triggers (mechanical stimulation, drug administration).

1. Introduction


Bone formation (osteogenesis) is a complex process in which i) cellular differentiation and ii) the generation of a mineralized organic matrix are synchronized to produce a hybrid hierarchical architecture.^[1] To study the molecular mechanisms of osteogenesis in health and disease, there is great need for functional self-organizing 3D model systems that capture in parallel, both cellular and matrix formation processes. Such a self-organizing 3D model system where mechanical and (bio)chemical signals can be applied in a dynamic environment, would be an important tool in the development of treatments for bone-related human diseases such as osteoporosis and osteogenesis imperfecta.

Organoids have been defined as “*in vitro* 3D cellular clusters derived exclusively from embryonic stem cells, induced pluripotent stem cells or primary tissue, capable of

Dr. A. Akiva, M. van Erp
Department of Cell Biology
Radboud Institute of Molecular Life Sciences
Radboud University Medical Center
Geert Grooteplein, Nijmegen, Gelderland 6525, The Netherlands
E-mail: anat.akiva@radboudumc.nl

Dr. A. Akiva, Dr. J. Melke, S. Ansari, Dr. F. Zhao, Prof. K. Ito,
Prof. N. Sommerdijk, Dr. S. Hofmann
Institute for Complex Molecular Systems (ICMS)
Eindhoven University of Technology
Eindhoven, North Brabant 5600, The Netherlands
E-mail: s.hofmann@tue.nl

Dr. A. Akiva, M. van Erp, Prof. N. Sommerdijk
Electron Microscopy Center
Radboud Institute of Molecular Life Sciences
Radboud University Medical Center
Geert Grooteplein, Nijmegen, Gelderland 6525, The Netherlands
E-mail: nico.sommerdijk@radboudumc.nl

 The ORCID identification number(s) for the author(s) of this article can be found under <https://doi.org/10.1002/adfm.202010524>.

© 2021 The Authors. Advanced Functional Materials published by Wiley-VCH GmbH. This is an open access article under the terms of the Creative Commons Attribution License, which permits use, distribution and reproduction in any medium, provided the original work is properly cited.

The copyright line for this article was changed on 27 April 2021 after original online publication.

DOI: 10.1002/adfm.202010524

Dr. A. Akiva, S. Ansari, R. van der Meijden, M. Stout, C. Muñiz Ortera,
Prof. N. Sommerdijk
Laboratory of Materials and Interface Chemistry
Department of Chemical Engineering and Chemistry
Eindhoven, North Brabant 5600, The Netherlands

Dr. J. Melke, S. Ansari, Dr. F. Zhao, Prof. K. Ito, Dr. S. Hofmann
Orthopaedic Biomechanics
Department of Biomedical Engineering
Eindhoven University of Technology
Eindhoven, North Brabant 5600, The Netherlands

Dr. N. Liv, C. de Heus, Dr. J. Fermie, Prof. J. Klumperman
Section Cell Biology
Center for Molecular Medicine
University Medical Center Utrecht
Utrecht, Utrecht 3584, The Netherlands

R. van der Meijden, Prof. N. Sommerdijk
Department of Biochemistry
Radboud Institute of Molecular Life Sciences
Radboud University Medical Center
Geert Grooteplein, Nijmegen, Gelderland 6525, The Netherlands

Dr. F. Zhao
Zienkiewicz Centre for Computational Engineering
College of Engineering
Swansea University
Swansea SA1 8EN, UK

Dr. W. H. Nijhuis
Department of Orthopaedic Surgery
University Medical Centre Utrecht
Wilhelmina Children's Hospital
Utrecht, Utrecht 3584, The Netherlands

self-renewal and self-organization, and exhibiting similar organ functionality as the tissue of origin”, where they may “rely on artificial extracellular matrices (ECM) to facilitate their self-organization into structures that resemble native tissue architecture”.^[2] As the development of organoids relies on their self-organizing nature, they also often show variability in their results. Nevertheless, currently organoids are those in vitro model systems that most closely resemble the in vivo situation in tissues and provide a promising approach toward personalized medicine. However, for human bone, no such functional organoid is yet available.

A crucial challenge here is the realization of a 3D system with different interacting bone cell types. In particular, the differentiation of human bone marrow-derived mesenchymal stromal cells (hBMSC) into osteocytes, which form 90–95% of the cellular fraction of bone tissue,^[3] has not yet been achieved in vitro and currently remains a critical step in the engineering of in vitro human bone models.

In vivo, osteocytes form through the differentiation of osteoblasts, after these become embedded in the extracellular matrix that they produce.^[3,4] Osteocytes are responsible for sensing the biophysical demands placed on the tissue and for orchestrating the concomitant actions of osteoblasts and osteoclasts in the remodeling of bone,^[1] as well as for maintaining calcium and phosphate homeostasis. During the differentiation from osteoblasts to osteocytes, the cells grow long extensions called processes, by which they form a sensory network that translates mechanical cues into biochemical signals and through which they interact with other cells.^[1]

In vitro, osteoblast-based cell lines developed as models of osteocytes or osteocyte differentiation have not yet been shown to produce a fully developed mineralized collagen matrix,^[5] and hence are limited in their function as 3D models for bone formation. So far, the full differentiation from mesenchymal stem cell (MSCs) into functional osteocytes has been demonstrated for mouse cells – and kept in culture for as long as a year^[6] – but this was not yet demonstrated for human cells. Recently, pre-osteocyte-like cells have been achieved from human primary cells,^[7] and co-cultures were generated from pre-prepared populations of osteoblasts and osteocytes.^[8] They have shown the production of the protein podoplanin – a marker for the embedding of osteocytes in a mineralizing matrix – over longer time periods, but the direct demonstration of the in vitro production of a 3D bone-like mineralized matrix showing intrafibrillar mineralization under biological control has not yet been demonstrated. Also missing is a demonstration of the production of sclerostin by osteocytes at the protein level, where sclerostin is a key anti-anabolic molecule that interacts with osteoblasts to down-regulate ECM formation. Hence, the creation of an organoid, as a model for developing bone, through the full differentiation of human primary cells into a functional osteocyte network within a bone-like mineralized matrix, is still an outstanding challenge.

As part of our efforts to realize a fully functional in vitro bone model, this work reports the differentiation of human BMSCs into a functional 3D self-organizing co-culture of osteoblasts and osteocytes, creating an organoid for early stage bone (woven bone) formation. We use a combination of immunohistochemistry, 2D and 3D electron microscopy and spectroscopy

to demonstrate that the osteocytes form a network showing cell–cell communication via the expression of sclerostin, embedded within the collagen matrix that is formed by the osteoblasts and mineralized under biological control.

With this extensive characterization, we demonstrate that this is the first fully functional 3D living in vitro model system for investigating the differentiation and matrix development processes during early bone formation.

2. Results

2.1. Differentiation of hBMSCs into a 3D Co-Culture of Osteoblast and Osteocytes

In the present work, primary hBMSCs were seeded on porous 3D silk fibroin scaffolds^[9] and subsequently cultured in osteogenic differentiation medium. The cells were exposed to mechanical stimulation through fluid flow derived shear stress, by applying continuous stirring in a spinner-flask bioreactor (Figure S1, Supporting Information), while a static system was used as control. Cells subjected to mechanical loading showed the production of a mineralized extracellular matrix (ECM) – as assessed by micro-computed tomography (μ CT) and histological staining for collagen, glycosaminoglycans, and minerals (Figure S2, Supporting Information). Fourier-transform infrared (FTIR) spectroscopy indicated a matrix composition similar to that of embryonic chicken bones (Figure S3, Supporting Information).^[10] In contrast, no significant ECM production was observed in the static system.

The histological sections also showed that the cells migrated within the scaffold, forming separated colonies. As these colonies present local environments, we expect the cells – as in any tissue – to show local variation in their degree of differentiation, related to differences in local mechanical stimulation, local cell density, scaffold shape or location within the scaffold.^[11] The simultaneous presence of several different developmental stages precludes monitoring cellular differentiation by standard genetic screening methods such as qPCR. The differentiation from primary cells to osteoblasts and osteocytes was therefore followed using immunohistochemistry, visualizing the expression of specific biomarkers at the protein level for the subsequent development to pre-osteoblasts, osteoblasts, and osteocytes (Figure 1; Figure S4, Supporting Information).^[1] The pre-osteoblastic stage was identified by the expression of transcription factors RUNX2 (CBFA-1) and osterix (OSX, SP7) (Figure 1a,b; Figure S4, Supporting Information). The next stage in the differentiation, the formation of osteoblasts, was heralded by the detection of osteoblast-specific markers, where alkaline phosphatase (ALP) was detected at the cell surfaces, and osteocalcin (BGLAP), osteopontin (BSP1), and osteonectin (SPARC) localized in the cellular environment (Figure 1c–f; Figure S4, Supporting Information). Finally, the differentiation into osteocytes was indicated by the expression of dentin matrix protein1 (DMP1), podoplanin (E11), and sclerostin (Figure 1g–i; Figure S4, Supporting Information). DMP1 is a marker for the early stages of osteocyte formation, coinciding with the embedding of the osteoblasts in the collagenous matrix. Podoplanin marks the osteocyte embedded in the non-mineralized matrix

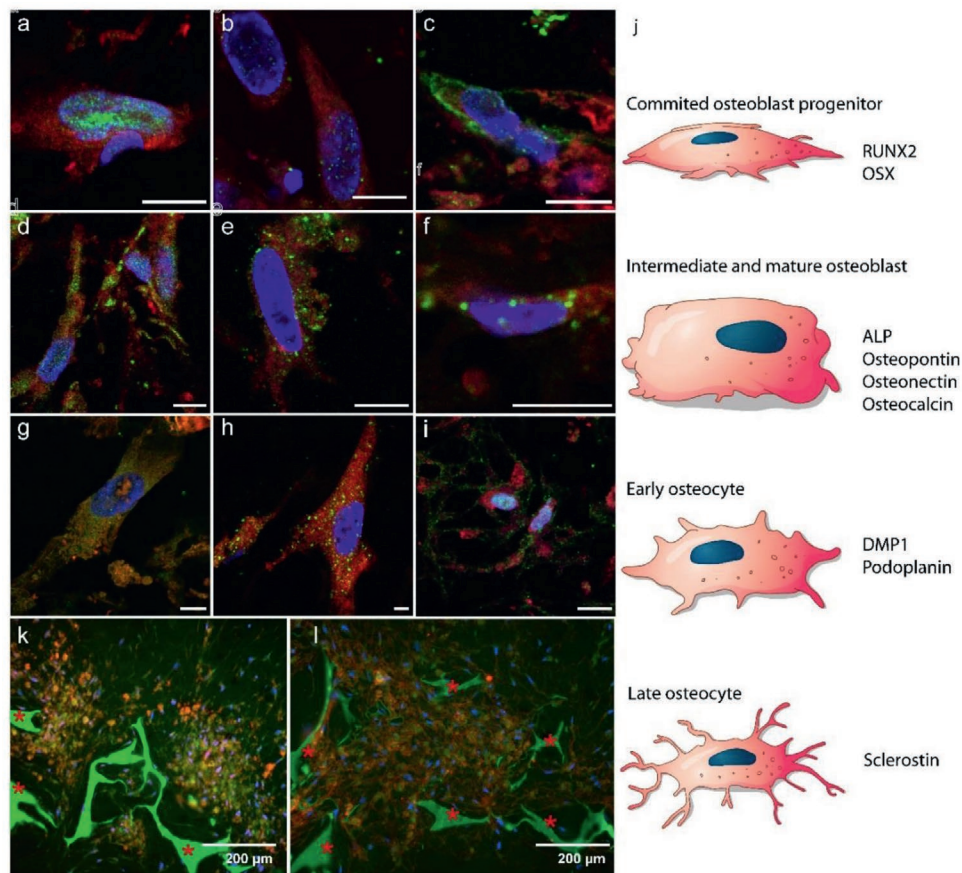


Figure 1. Differentiation of hBMSCs into osteoblasts and osteocytes: a–i) Fluorescence immunohistochemistry imaging showing markers for a–c) early stages of osteoblast formation, d–f) mature osteoblasts, and g–i) osteocyte development (5.55 mM glucose). Color code: red – cell cytoplasm, blue – cell nuclei, green: a) RUNX2 (day 7), b) OSX (day 7), c) ALP (day 26), d) osteocalcin (day 26), e) osteopontin (day 26), f) osteonectin (day 21), g) DMP1 (day 28), h) podoplanin (day 28), and i) sclerostin (day 28). Scale bars: 10 μm . See Figure S4, Supporting Information, for separate channels. j) Schematic illustration of MSCs differentiation into osteoblasts and osteocytes, indicating at which state which protein expression is expected in a–i. k, l) Fluorescent images indicating self-organized domains of osteocytes embedded in a mineralized matrix after 8 weeks (25 mM glucose), k) co-localization of osteocytes (sclerostin, red) and mineral (calcein, green), and l) collagen (CNA35, red) and mineral (calcein, green) * Indicates the silk fibroin scaffold.

stage and has been suggested to regulate cell process formation.^[3] Sclerostin indicates the maturation of the osteocytes and their ability to perform their signaling function in the bone regulatory process.^[11,12] We note that the rate of osteocyte differentiation depended not only on the exposure to mechanical stimulation, but also on the glucose concentration in the medium, as indicated by the detection of sclerostin after ≈ 4 weeks for 5.55 mM glucose (Figure 1i) and ≈ 8 weeks for 25 mM glucose (Figure 1k).

We then used fluorescence microscopy to investigate the ability of the cells to self-organize and form a mineralized ECM. Staining of the mineral with calcein showed the co-localization with sclerostin in large domains with dimensions of hundreds of micrometers, indicating the embedding of the osteocytes in a mineralized ECM (Figure 1k). Combined staining with calcein (mineral) and CNA35 (collagen) confirmed the presence of sub-millimeter sized mineralized collagen domains (Figure 1l) in the pores of the scaffold throughout its entire volume. These mineralized domains co-existed with non-mineralized domains that stained positive for osteoblast markers (Figure S5, Supporting Information).

This implies that a co-culture had formed in which osteogenic cells had organized themselves according to their stage of differentiation and maturation, and in which the osteocytes had become embedded within the mineralized matrix also produced by the system.

2.2. Osteocyte Network Analysis

Although the detection of DMP1, podoplanin and sclerostin markers indicated the presence of osteocytes in the co-culture, these observations do not prove that they form a connected functional network of cells. Fluorescence microscopy however confirmed the typical osteocyte morphology (Figure 2), showing the development of cell processes of >10 micrometer, as well as the formation of an interconnected network (Figure 2a; Figure S6, Supporting Information). Additionally, 3D focused ion beam/scanning electron microscopy (3D FIB/SEM) showed that the cells form a relatively dense 3D network with significant variation in their morphologies, as well as in the number, length, and

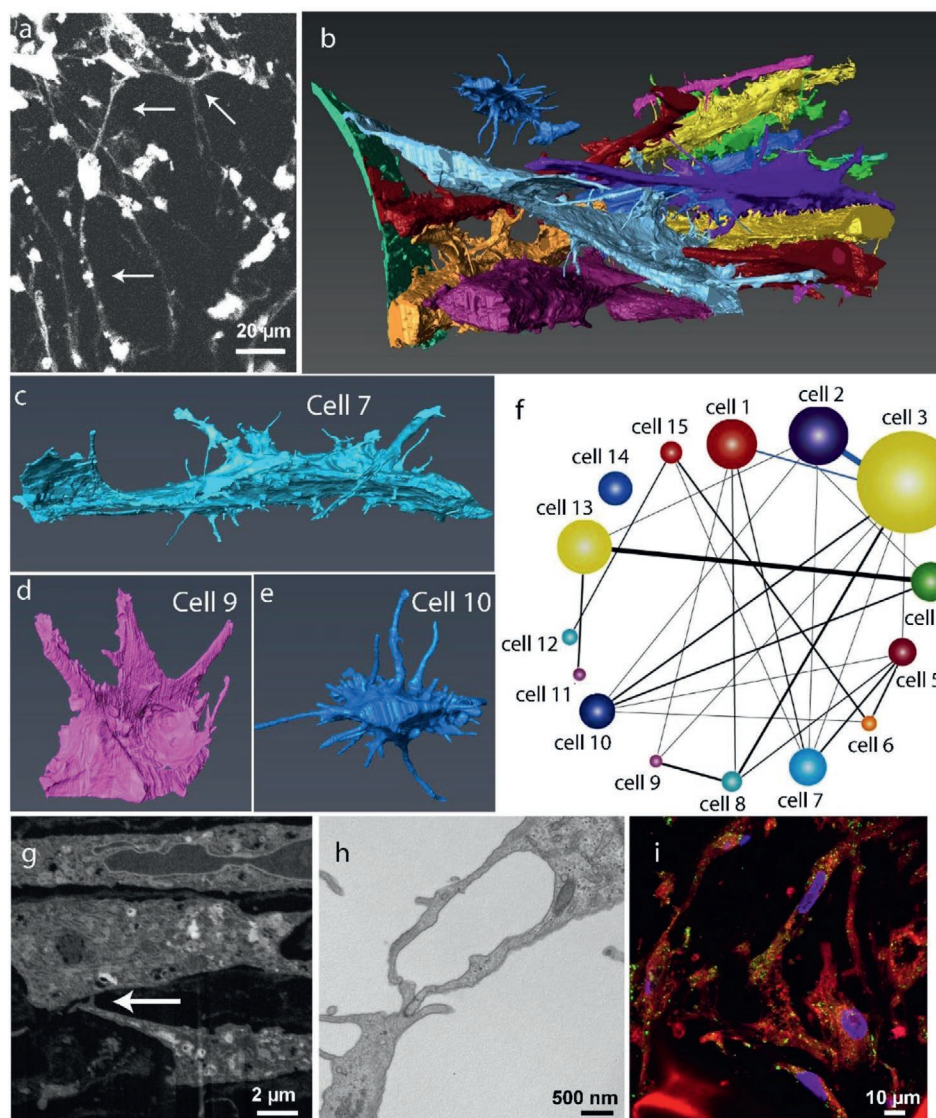


Figure 2. Osteocyte development and network formation. a) Fluorescent cytoplasm staining showing the development of long (>5 μm , arrows) cell processes connecting cells, and the formation of an interconnected network. The long processes were enhanced using a gamma value of -1.5 . (see original image in Figure S6, Supporting Information). b) 3D FIB/SEM reconstruction showing cell morphology and network formation in the whole volume. c–e) Details from the 3D reconstruction in (b) showing individual osteocytes in different stages of morphological development (cell numbers refer to identification in Figure S7, Supporting Information). c) Cell #7, d) cell #9, e) cell #14. f–i) Cell connectivity: f) Connectivity map of the cells in the 3D FIB/SEM stack (see also Tables S1 and S2, Supporting Information). Sizes of the circles reflect the number of processes of that respective cell. Thickness of the lines reflects the number of connections between individual cells (cell numbers refer to identification in Figure S7, Supporting Information). g) single slice from the 3D FIB/SEM stack showing long processes (arrow), creating a cellular network. h) TEM image shows a gap junction between processes of two connecting cells. i) fluorescent immunohistochemistry showing the presence of gap junctions on the surface of the different cells. Color code: red – cell cytoplasm, blue – cell nuclei, green – connexin43.

connectivity of their processes (Figure 2b–e; Tables S1 and S2, Supporting Information). We note that our osteocytes most often show flattened morphologies, which differ from those in text books with generally spherical or oblate bodies and long homogeneous protrusions, but are similar to osteocyte morphologies observed in different bone types, including rat tibia,^[13] human femur,^[14] and mouse woven bone.^[15]

Cells showed both connected and unconnected processes, with connections to 1–7 neighboring cells (Figure 2f; Figure S7 and Table S2, Supporting Information). The network had a

density of $750\,000\text{ cells mm}^{-3}$, which is higher than observed for mature osteocytes in cortical bone ($20\,000\text{--}80\,000\text{ cells mm}^{-3}$),^[4] but in line with numbers found for woven bone such as in embryonic chicken tibia ($500\,000\text{--}700\,000\text{ cells mm}^{-3}$).^[16] Image analysis (Figure S8, Supporting Information) shows that for the different cells, the number of processes per unit surface area ranged between $0.05\text{--}0.23\ \mu\text{m}^{-2}$ (Table S3, Supporting Information), in line with values reported for mouse osteocytes ($0.08\text{--}0.09\ \mu\text{m}^{-2}$).^[17] The functionality of the processes was indicated not only by their connection to neighboring cells

(Figure 2g,h), but also by their co-localization with connexin43, a protein essential for gap junction communication (Figure 2i).^[1] The observed variation in osteocyte morphology, together with the variation in the number of cell processes per surface area reflects the different stages of development and maturation, as expected in a differentiating osteogenic co-culture.

Hence, the osteocytes in our 3D in vitro system not only have the ability to organize themselves as a connective cellular network within a mineralized collagen matrix, but also show the capability to perform cell–cell communication.

2.3. Characterization of the Extracellular Matrix

Although it is essential that a 3D in vitro model for bone formation shows the relevant developmental stages, self-organization and cell–cell communication, its physiological relevance critically depends on its capability to reproduce the bone extracellular matrix. The formation and maintenance of a collagen–mineral hybrid tissue in vitro has previously been demonstrated using second harmonic generation imaging,^[18] Raman spectroscopy,^[19] and X-ray based techniques.^[20] Here, we therefore investigated the ability of our living in vitro system to form a functional ECM, in which collagen is mineralized under biological control (Figure 3).

FIB/SEM volume imaging with 3D reconstruction showed that the osteocytes were fully embedded in their ECM (Figure 3a; Video S1, Supporting Information). The produced collagen matrix enveloped the cells, but showed a low degree of long range order (Figure 3b), as known for woven bone.^[15,21] and in line with what was described for collagen layers containing osteocytes.^[22] The extracellular deposition of non-collagenous proteins (NCPs) was evidenced by immunohistochemical analysis, showing the presence of osteocalcin, osteopontin, and DMP1 and their co-localization with collagen (Figure 3c,d; Figure S9, Supporting Information).

Whereas μ CT (Figure S2, Supporting Information), FTIR (Figure S3, Supporting Information), histochemistry (Figure S2, Supporting Information), and fluorescence microscopy (Figure 1k) all indicated the mineralization of the organic matrix, none of these methods can provide the spatial resolution to demonstrate whether the mineral crystals are indeed, as in bone, co-assembled with the collagen fibrils,^[23] and not just the result of uncontrolled precipitation.^[24] We therefore applied a multiscale imaging approach to verify that matrix mineralization indeed occurred under biological control. Raman microspectroscopy of the extracellular matrix showed the spectral signature of developing bone (Figure 3f) and confirmed the co-localization of the mineral with the collagen (Figure S10, Supporting Information). Spectral analysis further confirmed that the mineral/matrix ratio (a key parameter for bone development, determined from the $\text{PO}_4 \nu_4/\text{Amide III}$ vibrations intensity ratio^[25]) in the co-culture was indeed in the range found for developing bone (Figure 3g).^[26]

At higher resolution (voxel size $10 \times 10 \times 20 \text{ nm}^3$), 3D FIB/SEM with back scatter detection revealed thin collagen fibrils (diameters 50–80 nm) with varying degrees of mineralization as also commonly observed in the early stages of bone development (Figure 3i; Video S2 and Figure S11, Supporting

Information).^[27] Applying a heat map presentation showed the coexistence of non-mineralized fibrils (blue) alongside a mineralized population (green-red range). Additionally, transmission electron microscopy (TEM) showed mineralized single fibrils,^[6a] indicating that the collagen matrix was indeed mineralized under biological control (Figure 3j).^[28] Nevertheless, in some areas also, larger mineral precipitates were observed (Figure S10 c, orange, Supporting Information) (Video S2, Supporting Information), possibly due to local non-biologically controlled precipitation of calcium phosphate.

3. Discussion

Woven bone is the first form of mammalian bone deposited during embryonic development and fracture, before being replaced by other bone types.^[21] This is typically the case in situations in which rapid formation is a prime concern, and where osteoclasts and bone remodeling do not yet play a role. Our results show the formation of a bone organoid consisting of a self-organized co-culture of osteoblasts and osteocytes representing a functional model for woven bone, an early state of bone formation in which the collagen matrix is still disorganized and distinct from the more mature ordered 3D structure.^[23] We demonstrate the functionality of the organoid by showing that the ECM formed by the osteoblasts is mineralized under biological control, and that the mature osteocytes self-organize into a network within the mineralized matrix where they express sclerostin and connexin43 at the protein level.

Interestingly, the production of sclerostin did not prohibit ECM formation throughout the organoid, suggesting that the down regulation of this process is a local effect. This may be explained by assuming the most mature osteocytes are in the center of the osteocyte domains, which would lead to a gradient of sclerostin decreasing towards the periphery of the network, only affecting the activity of the osteoblasts closest to the osteocyte domain.

The use of silk fibroin as a scaffold material rather than the frequently used collagen scaffolds, permits to differentiate between the supplied and the newly formed matrix material, and study the quality of the collagen matrix as function of external stimuli (mechanical load, therapeutics) or genetic diseases (e.g., osteogenesis imperfecta). The application of mechanical stimulation during the development of our stem cell based co-culture proved crucial for the osteogenic differentiation, and underlines the importance of the integration of self-organizing stem cell based strategies with environmental control in microfluidic systems in the recent organoid-on-a-chip approaches.^[29]

4. Conclusion

Summarizing, we conclude that we have generated an organoid for woven bone. The ability of this self-organizing 3D co-culture of osteoblasts and osteocytes to form an organic matrix that is mineralized under biological control, is currently the most complete human in vitro model system for bone formation. It introduces the ability to closely monitor both cellular and matrix formation processes and will thereby provide new unique possibilities for the study of genetic bone related diseases, and the development of personalized medicine.

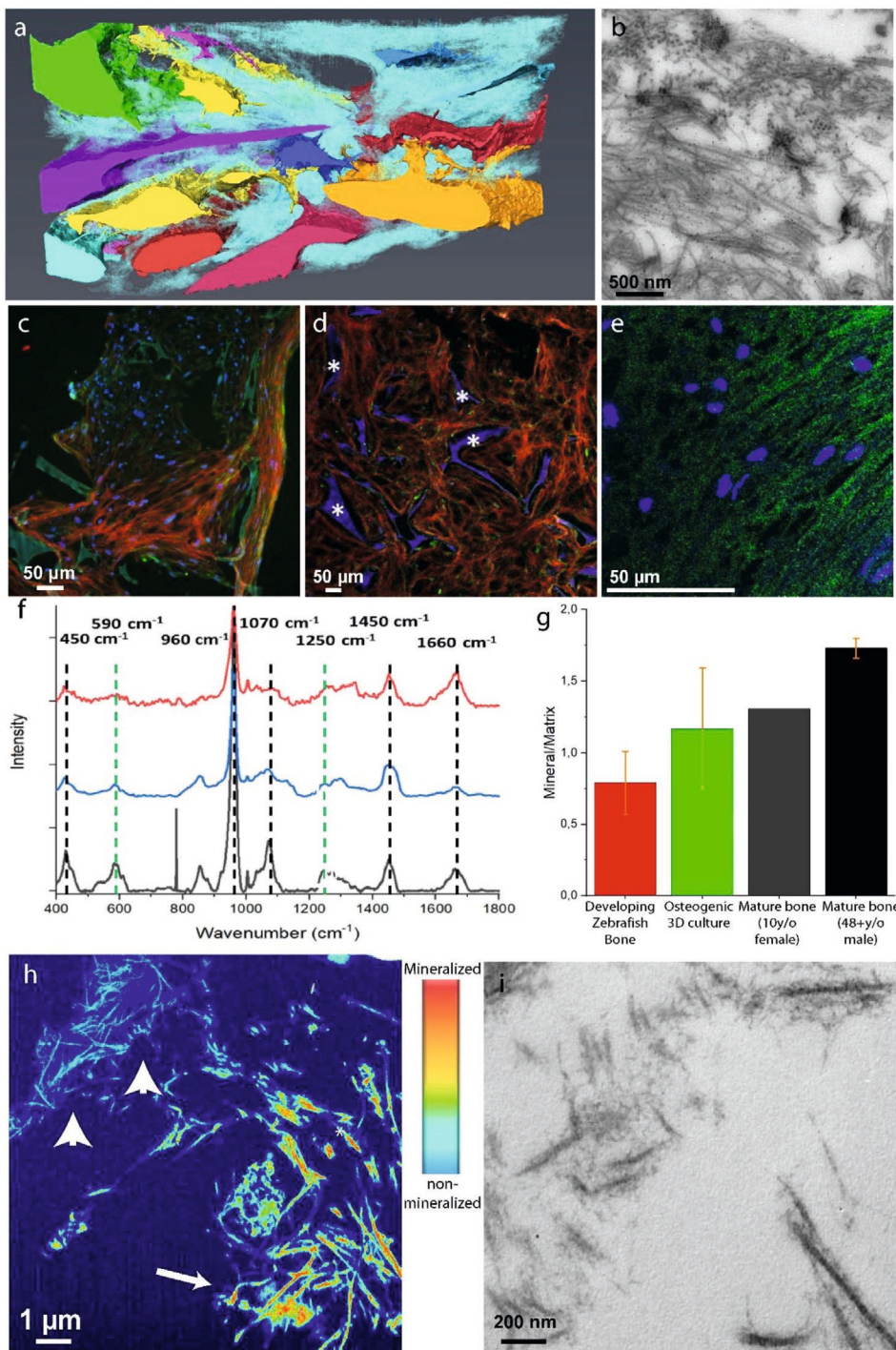


Figure 3. ECM development: a) 3D FIB/SEM reconstruction shows the embedding of the cells in the collagen matrix (cyan). Discrete cells are represented with different colors. b) TEM image of a 70 nm section showing the random distribution of collagen fibrils. Collagen type I was identified by immunolabelling. c–e) Fluorescent immunohistochemistry identifying key non-collagenous proteins in the collagenous matrix: c) Co-localization of osteocalcin (green) and collagen (red). d) Osteopontin (green) distribution in the collagen matrix (red). * Indicates the silk fibroin scaffold. e) Co-localization of DMP1 (green) with the collagen structure (see Figure S5, Supporting Information, for collagen image). f–g) Raman microspectrometry of mineralized matrices. f) Localized Raman spectra of mineralized collagen of developing zebrafish bone (red), the 3D osteogenic co-culture (blue), and human bone of a 10 year old female (grey g) Raman derived mineral/matrix ratios of 4 mineralized tissues of zebrafish ($N = 6$, red), Osteogenic 3D culture ($N = 7$, green), 10 year old human female ($N = 1$, grey), and 48+ years old human male ($N = 7$, black, taken from ref. [36]). Bars indicate sample standard deviations. h) Heat map presentation of a 3D FIB/SEM cross section showing disorganized collagen fibrils with different degrees of mineralization (Figure S10, Supporting Information). Arrowheads indicate non-mineralized collagen fibrils (light blue), arrow indicates mineralized collagen fibril (orange). i) TEM image showing individual mineralized collagen fibrils.

5. Experimental Section

Materials: Dulbecco's modified Eagle medium (DMEM high glucose Catalogue No. 41 966 and low glucose Cat. No. 31 885) and antibiotic/antimycotic (Anti-Anti) were from Life Technologies (Bleiswijk, The Netherlands). Citrate buffer was from Thermo Fisher Scientific (Breda, The Netherlands). Methanol was from Merck (Schiphol-Rijk, The Netherlands). Trypsin-EDTA (0.25%) was from Lonza (Breda, The Netherlands). Fetal bovine serum (FBS) was from PAA Laboratories (Cat. No A15-151, Cölbe, Germany). 10-nm Au particles conjugated to Protein-A were from CMC, UMC Utrecht (Utrecht, The Netherlands). BSA-c was from Aurion (Wageningen, The Netherlands). Silkworm cocoons from Bombyx mori L. were purchased from Tajima Shoji Co., LTD. (Yokohama, Japan). All other substances were of analytical or pharmaceutical grade and obtained from Sigma-Aldrich (Zwijndrecht, The Netherlands). The reference human bone sample used for Raman micro-spectrometry was waste material from a surgical procedure on a fractured left tibia of a 10-year-old female. According to the Central Committee on Research involving Human Subjects (CCMO), this type of study does not require approval from an ethics committee in the Netherlands (see <https://english.ccmo.nl/investigators/legal-framework-for-medical-scientific-research/your-research-is-it-subject-to-the-wmo-or-not>). Information on the embryonic chicken bone and zebrafish bone was gathered from ref. [15] (Kerschitzky et al.) and ref. [23] (Akiva et al.), respectively.

Scaffold Fabrication: Silk fibroin scaffolds were produced as previously described.^[30] Briefly, Bombyx mori L. silkworm cocoons were degummed by boiling in 0.2 M Na₂CO₃ twice for 1 h. The dried silk was dissolved in 9 M LiBr and dialyzed against ultra-pure water (UPW) for 36 h using SnakeSkin Dialysis Tubing (molecular weight cutoff: 3.5 K; Thermo Fisher Scientific, Breda, The Netherlands). Dialyzed silk fibroin solution was frozen at -80 °C and lyophilized (Freezone 2.5, Labconco, Kansas City, MO, USA) for 4 days, then dissolved in hexafluoro-2-propanol, resulting in a 17% (w/v) solution. Dissolved silk fibroin (1 mL) was added to NaCl (2.5 g) with a granule diameter of 250–300 μm and was allowed to air dry for 3 days. Silk-salt blocks were immersed in 90% MeOH for 30 min to induce β-sheet formation.^[31] NaCl was extracted from dried blocks in UPW for 2 days. Scaffolds were cut into disks of 5 mm in diameter and 3 mm in height and autoclaved in PBS at 121 °C for 20 min.

Cell Culture: Cells were isolated from unprocessed, fresh, human bone marrow (Lonza, Walkersville, MD, USA, cat. No #1M-125) of one male donor (healthy, non-smoker). hBMSCs isolation and characterization was performed as previously described and passaged up to passage 4.^[30] Pre-wetted scaffolds were seeded with 1 million cells each in 20 μL control medium (DMEM, 10% FBS, 1% Anti-Anti) and incubated for 90 min at 37 °C. The cell-loaded scaffolds were transferred to custom-made spinner flask bioreactors (*n* = 4 per bioreactor, Figure S1, Supporting Information). Each bioreactor contained a magnetic stir bar and was placed on a magnetic stirrer (RTV5, IKA, Germany) in an incubator (37 °C, 5% CO₂). Each bioreactor was filled with 5 mL osteogenic medium (control medium, 50 μg.mL⁻¹ ascorbic-acid-2-phosphate, 100 nM dexamethasone, and 10 mM β-glycerophosphate) and medium was changed three times a week.

Micro-Computed Tomography Imaging (μCT): μCT measurements and analysis were performed on a μCT100 imaging system (Scanco Medical, Brüttsellen, Switzerland). Scanning of the co-culture samples within the bioreactor was performed at an isotropic nominal resolution of 17.2 μm, energy level was set to 45 kVp, intensity to 200 μA, 300 ms integration time and twofold frame averaging. A constrained Gaussian filter was applied to reduce part of the noise. Filter support was set to 1.0 and filter width sigma to 0.8 voxel. Filtered grayscale images were segmented at a global threshold of 23% of the maximal grayscale value to separate the mineralized tissue from the background and binarize the image. Unconnected objects smaller than 50 voxels were removed and neglected for further analysis. Quantitative morphometrical analysis was performed to assess mineralized ECM volume within the entire scaffold volume using direct microstructural bone analysis as previously described for human bone biopsies.^[32]

Histological Analysis: Fixation and Sectioning: Co-cultures were fixed in 10% neutral buffered formalin (24 h at 4 °C), dehydrated in serial ethanol solutions (50%, 70%, 90%, 96%, 100%, 100%, 100%), embedded in paraffin, cut into 6 μm thick sections and mounted on Poly-L-Lysine coated microscope slides. Paraffin sections were dewaxed with xylene and rehydrated to water through graded ethanol solutions.

Brightfield Imaging: Sections were stained with Alizarin Red to identify mineralization (2%, Sigma-Aldrich), Picosirius Red (0.1%, Sigma-Aldrich) to identify collagen, Alcian blue (1%, Sigma-Aldrich) to identify Glycosaminoglycan (GAGs). Sections were imaged using Zeiss Axio Observer Z1 microscope.

Immunohistochemistry: Antigen retrieval in pH 6 citrate buffer at 95 °C was performed for 20 min. Sections were washed three times in PBS. Non-specific antibody binding was blocked with 5% serum (v/v) from the host of the secondary AB and 1% bovine serum albumin (w/v) in PBS (blocking buffer) for 1 h. Sections were then incubated overnight at 4 °C with primary antibodies in blocking buffer. The sections were rinsed with PBS four times for 5 min and incubated for 1 h with secondary antibodies in blocking buffer and at times with calcein solution (1 μg.mL⁻¹, C0875 Sigma-Aldrich). All used antibodies and dyes are listed in **Table 1**. Nuclei were stained with DAPI for 5 min, after which sections were again washed three times with PBS and mounted on microscope glass slides with Mowiol. Cytoplasm was stained with FM 4-64 (Molecular Probes cat#T3166) for 1 min and followed by washing the sections three times with PBS. Except for primary antibody incubation, all incubation steps were performed at room temperature. Sections were imaged either by Zeiss Axiovert 200M microscope (large field of view) or by Leica TCS SP5X (x63, high magnification images). Images were post processed (brightness, contrast, channel merging, and crop) using Fiji software.

Electron Microscopy: Sample Preparation for Electron Microscopy: Samples were processed for electron microscopy as previously described.^[33] In short, co-culture samples were fixed in 2.5% glutaraldehyde and 2% paraformaldehyde in 0.1 M sodium cacodylate buffer (CB) for 72 h and washed five times in 0.1 M CB and five times in double-distilled water (ddH₂O). Co-cultures were then post fixed using 1% OsO₄ with 0.8% K₃Fe(CN)₆ in 0.1 M CB for 1 h on ice. After rinsing in 0.1 M CB, the co-cultures were treated with 1% tannic acid followed by 1% uranyl acetate in ddH₂O for 1 h. Finally, the samples were rinsed using ddH₂O, dehydrated with ethanol (50%, 70%, 90%, 96%, 100%), and embedded in Epon resin.

Focused Ion Beam Scanning Electron Microscopy (FIB/SEM) Imaging: Epon embedded samples were imaged with a Scios FIB/SEM (Thermo Fisher Scientific, Breda, The Netherlands) under high vacuum conditions. Using the gas injection system (GIS) in the FIB/SEM microscope, a 500 nm thick layer of Pt was deposited over the ROI, at an acceleration voltage of 30 kV and a current of 1 nA. Trenches flanking the ROI were milled at an acceleration voltage of 30 kV, using a high FIB beam current (5–7 nA), followed by a staircase pattern in front of the ROI to expose the imaging surface. Fine polishing was performed with the ion beam set to 30 kV with a FIB beam current of 0.5 nA, resulting in a smooth imaging surface. Serial imaging was then performed using the in-column backscattered electron detector, and the following settings: Acceleration voltage 2 kV, Beam current 0.2 nA, Pixel dwell time 10 μs, voxel size: 30 × 30 × 30 nm (stack in Video S1, Supporting Information) and 10 × 10 × 20 nm (stack in Video S2, Supporting Information).

Sample Preparation for Transmission Electron Microscopy (TEM): Epon embedded samples: 70 nm sections from resin embedded blocks were made using an ultra-microtome (Leica), and collected on carbon coated copper TEM grids. Post staining with uranyl acetate and lead citrate was performed using the Leica EM AC20 automatic contrasting instrument.

Preparation and Immunogold Labeling of Tokuyasu Sections: Thin sections were prepared following the Tokuyasu protocol.^[34] Briefly, co-cultures were fixed as described above and infiltrated overnight in 2.3 M sucrose for cryo-protection. Small blocks of the co-cultures were mounted on aluminum pins and plunge frozen in liquid nitrogen. 70 nm thick cryosections were sectioned with a cryo-ultramicrotome and picked up with a mixture of 2% methylcellulose/2.3 M sucrose on copper support grids coated with formvar and carbon. After rinsing away the

Table 1. List of all antibodies and dyes used.

Antigen	Source	Catalogue No	Label	Species	Dilution/concentration
ALP	Thermo Fisher	MA5-17030	—	Mouse	1:200
Calcein Green	Sigma	C0875	—	—	1 $\mu\text{g.mL}^{-1}$
CNA35-mCherry	Homemade ^[37]	—	mCherry	—	1 μM
Collagen1	Abcam	ab34710	—	Rabbit	1:250
Connexin 43	Sigma	C6219	—	Rabbit	1:500
DAPI	Sigma	D9542	—	—	0.1 $\mu\text{g.mL}^{-1}$
DMP1	biobyte	orb247330	—	Rabbit	1:400
FM 4–64	Molecular Probes	T3166	—	—	5 $\mu\text{g.mL}^{-1}$
Osteocalcin	Abcam	Ab93876	—	Rabbit	1:200
Osteonectin	Thermo Fisher	MA1-43027	—	Mouse	1:500
Osteopontin	Thermo Fisher	14-9096-82	—	Mouse	1:200
OSX	Abcam	ab22552	—	Rabbit	1:200
Podoplanin	Abcam	ab128994	—	Rabbit	1:200
RUNX2	Abcam	Ab23981	—	Rabbit	1:500
Sclerostin	Thermo Fisher	PA5-37943	—	Goat	1:200
Goat IgG (H+L)	Jackson Immuno	A11055	Alexa 488	Donkey	1:200
Mouse IgG (H+L)	Molecular Probes	A21236	Alexa 647	Goat	1:200
Mouse IgG (H+L)	Jackson Immuno	715-545-150	Alexa 488	Donkey	1:200
Rabbit IgG (H+L)	Invitrogen	A21206	Alexa 488	Donkey	1:200
Rabbit IgG (H+L)	Molecular Probes	A21244	Alexa 647	Goat	1:200
Alizarin Red	Sigma–Aldrich	A5533	—	—	2%
Picrosirius Red	Sigma–Aldrich	365 548	—	—	0.1%
Alcian blue	Sigma–Aldrich	A5268	—	—	1%

pick-up solution in PBS at 37 °C for 30 min, the sections were treated with PBS containing 0.15% glycine, followed by blocking for 10 min with 0.5% cold fish skin gelatin and 0.1% BSA-c in PBS. The TEM grids were incubated for 1 h with a collagen type 1 antibody in blocking solution (Abcam, AB34710). The grids were then rinsed with 0.1% BSA in PBS and incubated with 10-nm Au particles conjugated to Protein-A in blocking solution.^[35] The sections were then thoroughly washed in ddH₂O, stained with uranyl acetate and embedded in methylcellulose.^[35]

TEM Imaging: The sections were imaged using a Tecnai T12 TEM (80kV) (Thermo Fisher Scientific, Breda, The Netherlands), equipped with Veleta (EMSIS GmbH, Münster, Germany).

Raman Spectroscopy: Raman measurements were conducted using a WiTec Alpha 300R confocal Raman microscope. Co-culture samples were fixed in 10% neutral buffered formalin (24 h at 4 °C), incubated for 2 h in 5% sucrose at 4 °C, embedded in Tissue-Tek (Sakura Finetek 4 609 024), cut into 10 μm thick sections, and mounted on Poly-L-Lysine coated microscope slides. Raman imaging was conducted using 532 nm excitation lasers with a laser power of 10 mW, using 50 \times 0.8 objective (0.8 NA) with a grating of 600 mm^{-1} . The maps were obtained with a spatial resolution of 3 $\text{spectra}.\mu\text{m}^{-1}$. Data analysis was performed using Project V plus software (Witec, Ulm) and Origin 8.

FTIR Spectroscopy: Prior to the FTIR measurement, the co-culture samples were freeze dried overnight. After drying, 1.5 mg of the samples was crushed using mortar and pestle until a fine powder was achieved. After this, 148.5 mg of KBr was added to the mortar and pestle and the materials were mixed and further crushed to a fine homogeneous mixture. The mixture was added to a pellet press holder; the transparent and homogeneous pellets were then inserted into the FTIR spectrometer (Perkin Elmer one 1600). The FTIR spectra were obtained in transmission mode. Spectra were obtained over the range from 200 to 6000 cm^{-1} with a spectral resolution of 0.5 cm^{-1} .

Image Analysis: 3D FIB/SEM Image processing was performed using Matlab and Avizo 3D software (FEI VSG, www.avizo3d.com). 3D image reconstruction, alignment, denoising, and brightness and contrast adjustments were done using Matlab. 3D segmentation was done using Avizo. Segmentation was performed using manual thresholding, and cell processes were counted manually. As all cells were only partially captured in the available FIB/SEM volume, cell process density was determined per unit surface area of the cell body. The surface areas of cell parts captured in the FIB/SEM volume were calculated from the segmented 3D image mask using Matlab and Fiji. Further details are given in Figure S11, Supporting Information.

Cell density was determined from the number of cells in the imaged FIB/SEM volume (20 μm \times 20 μm \times 40 μm) and compared to literature data from histological sections (volume 5 μm \times 1000 μm \times 1000 μm).^[16]

Supporting Information

Supporting Information is available from the Wiley Online Library or from the author.

Acknowledgements

A.A. and J.M. contributed equally to this work. The authors would like to thank Lia Addadi and Steve Weiner for providing the zebrafish and embryonic chicken data, the ICMS animation studio (Koen Pieterse) for the graphics of the cells, and Carlijn Bouten for providing CNA35 collagen probe. The authors also thank Deniz Daviran for her help in preparing the figures. A.A. was supported by the Marie Curie Individual Fellowship

(H2020-MSCA-IF-2017-794296-SUPERMIN), by the Netherlands Organization for Scientific Research (NWO) through an ECHO grant to NS, and by the National Postdoctoral Award Program for Advancing Women in Science – the Weizmann Institute of Science, Israel. N.S., R.v.d.M. and M.v.E. were supported by the European Research Council (ERC) Advanced Investigator grant (H2020-ERC-2017-ADV-788982-COLMIN) to N.S. S.A. was supported by the Ministry of Education, Culture and Science (Gravitation Program 024.003.013). N.L. was supported by the Netherlands Organization for Scientific Research (NWO) through a ZonMW-TOP grant to J.K. J.M., F.Z., and S.H. were supported by the ERC Starting grant (FP7-ERC-2013-StG-336043-REMOTE) to SH.

Conflict of Interest

The authors declare no conflict of interest.

Data Availability Statement

Research data are not shared.

Keywords

3D cell culture, 3D electron microscopy, biomineralization, bone model, organoid

Received: December 7, 2020

Revised: February 7, 2021

Published online: March 9, 2021

- [1] *Principles of Bone Biology*, (4th ed.), (Eds: J. P. Bilezikian, T. J. Martin, T. L. Clemens, C. J. Rosen), Academic Press, Waltham, MA **2020**, pp. 1943–1986.
- [2] A. Fatehullah, S. H. Tan, N. Barker, *Nat. Cell Biol.* **2016**, *18*, 246.
- [3] L. F. Bonewald, *J. Bone Miner. Res.* **2011**, *26*, 229.
- [4] T. A. Franz-Odenaal, B. K. Hall, P. E. Witten, *Dev. Dyn.* **2006**, *235*, 176.
- [5] C. Zhang, A. D. Bakker, J. Klein-Nulend, N. Bravenboer, *Curr. Osteoporosis Rep.* **2019**, *17*, 207.
- [6] a) K. Wang, L. Le, B. M. Chun, L. M. Tiede-Lewis, L. A. Shiflett, M. Prideaux, R. S. Campos, P. A. Veno, Y. Xie, V. Dusevich, L. F. Bonewald, S. L. Dallas, *J. Bone Miner. Res.* **2019**, *34*, 979; b) A. Iordachescu, H. D. Amin, S. M. Rankin, R. L. Williams, C. Yapp, A. Bannerman, A. Pacureanu, O. Addison, P. A. Hulley, L. M. Grover, *Adv. Biosyst.* **2018**, *2*, 1700156.
- [7] a) G. Thirivikraman, A. Athirasala, R. Gordon, L. Zhang, R. Bergan, D. R. Keene, J. M. Jones, H. Xie, Z. Chen, J. Tao, B. Wingender, L. Gower, J. L. Ferracane, L. E. Bertassoni, *Nat. Commun.* **2019**, *10*, 3520; b) G. Nasello, P. Alamán-Díez, J. Schiavi, M. Á. Pérez, L. McNamara, J. M. García-Aznar, *Front. Bioeng. Biotechnol.* **2020**, *8*, 336.
- [8] J. Skottke, M. Gelinsky, A. Bernhardt, *Int. J. Mol. Sci.* **2019**, *20*, 1998.
- [9] J. R. Vetsch, S. J. Paulsen, R. Muller, S. Hofmann, *Acta Biomater.* **2015**, *13*, 277.
- [10] M. Kerschnitzki, A. Akiva, A. Ben Shoham, Y. Asscher, W. Wagermaier, P. Fratzl, L. Addadi, S. Weiner, *J. Struct. Biol.* **2016**, *195*, 82.
- [11] J. Melke, F. Zhao, B. van Rietbergen, K. Ito, S. Hofmann, *Eur. Cells Mater.* **2018**, *36*, 57.
- [12] R. L. v. B. Kenneth, E. S. Poole, N. Loveridge, H. Hamersma, C. W. L. Socrates, E. Papapoulos, J. Reeve, *FASEB J.* **2005**, *19*, 1842.
- [13] S. W. Verbruggen, T. J. Vaughan, L. M. McNamara, *J. R. Soc., Interface* **2012**, *9*, 2735.
- [14] P. Varga, B. Hesse, M. Langer, S. Schrof, N. Mannicke, H. Suhonen, A. Pacureanu, D. Pahr, F. Peyrin, K. Raum, *Biomech. Model. Mechanobiol.* **2015**, *14*, 267.
- [15] M. Kerschnitzki, W. Wagermaier, P. Roschger, J. Seto, R. Shahar, G. N. Duda, S. Mundlos, P. Fratzl, *J. Struct. Biol.* **2011**, *173*, 303.
- [16] R. Yair, A. Cahaner, Z. Uni, R. Shahar, *Poult. Sci.* **2017**, *96*, 2301.
- [17] D. Tokarz, R. Cisek, M. N. Wein, R. Turcotte, C. Haase, S. A. Yeh, S. Bharadwaj, A. P. Raphael, H. Paudel, C. Alt, T. M. Liu, H. M. Kronenberg, C. P. Lin, *PLoS One* **2017**, *12*, e0186846.
- [18] a) R. M. Delaine-Smith, S. MacNeil, G. C. Reilly, *Eur. Cells Mater.* **2012**, *24*, 162; b) C. Brackmann, M. Zaborowska, J. Sundberg, P. Gatenholm, A. Enejder, *Tissue Eng., Part C* **2012**, *18*, 227.
- [19] A. A. van Apeldoorn, Y. Aksenov, M. Stigter, I. Hofland, J. D. de Bruijn, H. K. Koerten, C. Otto, J. Greve, C. A. van Blitterswijk, *J. R. Soc., Interface* **2005**, *2*, 39.
- [20] M. Mastrogiacomo, V. S. Komlev, M. Hausard, F. Peyrin, F. Turquier, S. Casari, A. Cedola, F. Rustichelli, R. Cancedda, *Tissue Eng.* **2004**, *10*, 1767.
- [21] S. W. and, H. D. Wagner, *Annu. Rev. Mater. Sci.* **1998**, *28*, 271.
- [22] N. Reznikov, R. Shahar, S. Weiner, *Bone* **2014**, *59*, 93.
- [23] N. Reznikov, R. Shahar, S. Weiner, *Acta Biomater.* **2014**, *10*, 3815.
- [24] B. W. M. de Wildt, S. Ansari, N. A. J. M. Sommerdijk, K. Ito, A. Akiva, S. Hofmann, *Curr. Opin. Biomed. Eng.* **2019**, *10*, 107.
- [25] M. Kazanci, P. Roschger, E. P. Paschalis, K. Klaushofer, P. Fratzl, *J. Struct. Biol.* **2006**, *156*, 489.
- [26] A. Akiva, M. Kerschnitzki, I. Pinkas, W. Wagermaier, K. Yaniv, P. Fratzl, L. Addadi, S. Weiner, *J. Am. Chem. Soc.* **2016**, *138*, 14481.
- [27] M. D. McKee, A. Nanci, *Microsc. Res. Tech.* **1995**, *31*, 44.
- [28] S. Weiner, W. Traub, *FEBS Lett.* **1986**, *206*, 262.
- [29] S. E. Park, A. Georgescu, D. Huh, *Science* **2019**, *364*, 960.
- [30] S. Hofmann, H. Hagenmuller, A. M. Koch, R. Muller, G. Vunjak-Novakovic, D. L. Kaplan, H. P. Merkle, L. Meinel, *Biomaterials* **2007**, *28*, 1152.
- [31] R. Nazarov, H.-J. Jin, D. L. Kaplan, *Biomacromolecules* **2004**, *5*, 718.
- [32] a) L. A. Hildebrand, T. Muller, R. Dequeker, J. Ruegsegger P, *J. Bone Miner. Res.* **1999**, *14*, 1167; b) G. H. van Lenthe, H. Hagenmuller, M. Bohner, S. J. Hollister, L. Meinel, R. Muller, *Biomaterials* **2007**, *28*, 2479.
- [33] J. Fermie, N. Liv, C. Ten Brink, E. G. van Donselaar, W. H. Muller, N. L. Schieber, Y. Schwab, H. C. Gerritsen, J. Klumperman, *Traffic* **2018**, *19*, 354.
- [34] a) S. T. Oorschot VMJ, R. J. Bryson-Richardson, G. Ramm, in *Correlative Light and Electron Microscopy. II*, Academic Press, Waltham, MA **2014**, pp. 241–258; b) E. van Meel, M. Boonen, H. Zhao, V. Oorschot, F. P. Ross, S. Kornfeld, J. Klumperman, *Traffic* **2011**, *12*, 912.
- [35] J. Slot, H. Geuze, *Nat. Protoc.* **2007**, *2*, 2480.
- [36] J. S. Nyman, A. J. Makowski, C. A. Patil, T. P. Masui, E. C. O'Quinn, X. Bi, S. A. Guelcher, D. P. Nicolletta, A. Mahadevan-Jansen, *Calcif. Tissue Int.* **2011**, *89*, 111.
- [37] K. N. Krahn, C. V. C. Bouten, S. van Tuijl, M. A. M. J. van Zandvoort, M. Merckx, *Anal. Biochem.* **2006**, *350*, 177.